Circuit Analysis and Defect Characteristics Estimation Method Using Bimodal Defect-Centric Random Telegraph Noise Model

Michitarou Yabuuchi[1], Azusa Oshima[1], Takuya Komawaki[1], Ryo Kishida[1], Jun Furuta[1],
Kazutoshi Kobayashi[1], Pieter Weckx[2,3], Ben Kaczer[3], Takashi Matsumoto[4], and Hidetoshi Onodera[5]

[1]Kyoto Institute of Technology, [2]KU Leuven, [3]IMEC, [4]University of Tokyo, and [5]Kyoto University

***Abstract*—We propose circuit analysis and defect characteristics estimation methods using the bimodal RTN (random telegraph noise) model of the defect-centric distribution. The bimodal model takes into account the defect characteristics of both high-k and interface layers in gate dielectrics on a 40 nm SiON process, whereas the conventional unimodal model fails to replicate the effects of RTN on the process. The estimation method calculates parameters of the defect characteristics of the bimodal model by using RTN-induced frequency fluctuations measured on the ring oscillators. The analysis method reproduces distributions of RTN-induced frequency fluctuations by the Monte Carlo simulation using the defect parameters. We confirm the proposed methods fully replicates the effect of RTN by comparing simulation and measurement results of a 40 nm test chip.**

***Keywords*—RTN (Random Telegraph Noise), defect-centric distribution, variation, reliability, circuit design**

I. Introduction

Dynamic variation such as RTN (Random Telegraph Noise) become to have a significant impact on reliability of semiconductor chips as comparable as static process variations on 40 nm or later processes [1]. Fig. 1 shows that physical origin of RTN is defects (traps) in gate dielectrics which capture and emit carriers in channels [2]. The mechanism of RTN is as same as that of BTI (Bias Temperature Instability) [3]. ΔV_{th} (threshold voltage shift) is used to model RTN on the transistor-level [4]. It has been reported that RTN has a serious impact on CMOS sensors and memories [5]–[7]. It is necessary for circuit designers to predict the impact of RTN to the circuit-level.

It is proposed that ΔV_{th} by the defects follows the defect-centric distribution [3]. It estimates the impact of RTN to the MOSFET operation by using N and η, where N is an expected value of the number of defects which capture carriers and η is an expected value of impacts to ΔV_{th} by each of the defects [8], [9]. MOSFETs fabricated on 40 nm or later process have HK (high-k layers) and IL (interface layers) in their gate dielectrics. In this case, distributions of ΔV_{th} of BTI are reproduced by 4 parameters, which are N and η of each layer [10]. RTN on the multi-layer process are also reproduced in the same way [11]. It is called "bimodal model" whereas conventional "unimodal model" only takes into account the defects in a single layer. Circuit designers have to consider impacts of RTN of the bimodal model in the scaling process. However, circuit analysis methods using the bimodal RTN model are not reported because of the difficulty of the prediction with the four parameters of the defect characteristics (N and η of each layer).

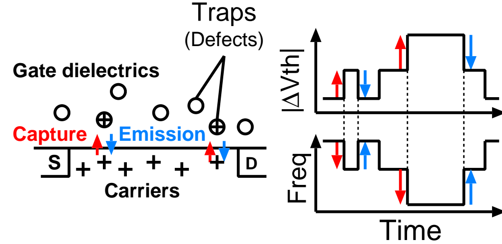

Fig. 1. RTN is caused by capture and emission of carriers at defects in gate dielectrics.

In this paper, a circuit-level modeling method of RTN by using the bimodal defect-centric model and a estimation method of the defect parameters are proposed. Our approach has two features as follows.

- Predict impacts of the bimodal RTN by using circuit analysis with the ΔV_{th} distribution
- Estimate the defect characteristics of each HK and IL by measurement results of a 40 nm test chip

RTN-induced variations are predicted by our proposed methods.

This paper is organized as follows. Section II shows the transistor-level modeling based on the physical origin of RTN, measurement results of the test chip, and the analysis method on the circuit-level. Section III introduces the estimation method of the defect characteristics and experiment results which compare the prediction with the measurement results. Section IV concludes this paper.

II. Transistor-Level Modeling and Circuit-Level Prediction Method

In this section, a transistor-level RTN model based on the physical origin, measurement results of RTN distribution on 40 nm test chips, and a circuit-level RTN prediction method are introduced.

A. Transistor-Level RTN Modeling

RTN-induced ΔV_{th} on a single MOSFET follows the defect-centric distribution which is based on the physical behavior of the defects [3]. Fig. 2 shows a mean value of ΔV_{th} is a product of N and η, where N is an expected value of the

number of the capturing defects and η is an expected value of $\Delta V_{\rm th}$ on each of the defects. N is expressed by Eq. (1) [12].

$$N = LWD \tag{1}$$

Where, D is a defect density which depends a fabricated process. N is proportional to the gate area LW, whereas η is inversely proportional to LW as shown in Eq. (2) [13].

$$\eta = \frac{s}{LW} \tag{2}$$

Where, s is a coefficient which is also a process parameter. The number of defects and $\Delta V_{\rm th}$ on each of the defects follow the Poisson and the exponential distribution, respectively. Therefore, the CDF (Cumulative Density Function) of $\Delta V_{\rm th}$ on MOSFETs is represented in Eq. (3).

$$F_{N,\eta}(\Delta V_{\rm th}) = \sum_{n=0}^{\infty} \frac{e^{-N} N^n}{n!} F_{n,\eta}(\Delta V_{\rm th}) \tag{3}$$

A mean value and a standard deviation of the defect-centric distribution are shown in Eqs. (4) and (5), respectively.

$$\mu_{\Delta \rm V_{th}} = N\eta \quad (= \text{constant}) \tag{4}$$

$$\sigma_{\Delta \rm V_{th}} = \sqrt{2N\eta^2} \quad (\propto 1/\sqrt{LW}) \tag{5}$$

From those equation, $\mu_{\Delta \rm V_{th}}$ is constant although the size of MOSFETs shrinks. However, $\sigma_{\Delta \rm V_{th}}$ becomes larger with scaling. Therefore, the RTN-induced $\Delta V_{\rm th}$ is distributed wider range in the smaller devices. In other words, the impacts of RTN on the circuits become crucial with the downscaling.

Fig. 3 shows three types of gate dielectric materials and models of the defect-centric distribution. The unimodal defect-centric distribution shown in Eq. (3) accurately predicts the RTN effects in (a) SiO_2/SiON and Poly-Si processes, but it is inapplicable in (b) Ultra thin HK/Poly-Si and (c) HKMG (high-k metal gate) processes [10]. RTN-induced $\Delta V_{\rm th}$ in (b) and (c) is characterized by two independent N and η attributed to the defects in the HK and the IL regions. The mean values of numbers of the defects in these regions are defined as $N_{\rm HK}$ and $N_{\rm IL}$. The mean values of the impacts of RTN to $\Delta V_{\rm th}$ per defect to RTN are defined as $\eta_{\rm HK}$ and $\eta_{\rm IL}$. A CDF of the bimodal defect-centric distribution is described as Eq. (6).

$$F_{N_1,N_2,\eta_1,\eta_2}(\Delta V_{\rm th}) = \sum_{n_1=0}^{\infty} \sum_{n_2=0}^{\infty} \frac{e^{-N_1} N_1^{n_1}}{n_1!} \frac{e^{-N_2} N_2^{n_2}}{n_2!} F_{n_1,n_2,\eta_1,\eta_2}(\Delta V_{\rm th}) \tag{6}$$

Note that subscripts 1 and 2 are corresponding to the HK and the IL. In this paper, the bimodal model is focused on.

B. Measurement of RTN on Test Chip

A method to measure RTN-induced frequency fluctuations on test chips and a method to evaluate the impact of RTN are explained in this section. The measurement results are used for the parameter estimation in Section III.

Fig. 4 shows the test structure which is a 7-stage RO (ring oscillator). The chip including the 840 ROs are fabricated in a 40 nm HK/Poly-Si process. The process has the HK region

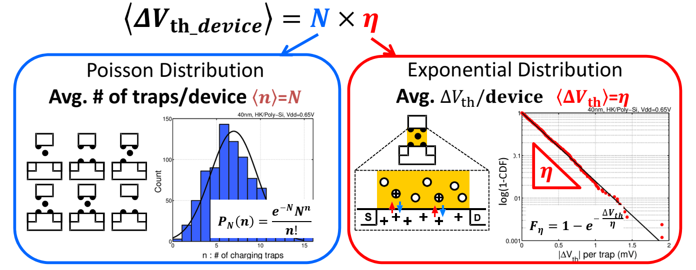

Fig. 2. Prediction of RTN-induced $\Delta V_{\rm th}$ on a single MOSFET.

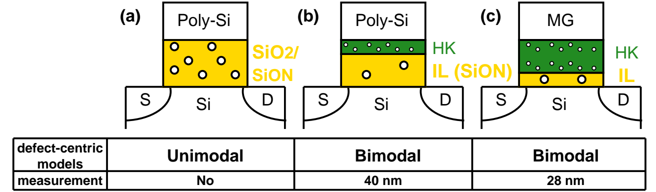

Fig. 3. Dielectric materials and two models of defect-centric distribution, (a) SiO_2/Poly-Si, (b) Ultra thin HK/Poly-Si, and (c) HKMG processes [11].

and is corresponding to (b) in Fig. 3. The HK region is doped to optimize the gate work function [14]. The RTN effects are observed as frequency fluctuations on measurements of the ROs. The method that measures the ROs collects the data more efficiently than that of transistors. This approach has the disadvantage that it fails to directly obtain $\Delta V_{\rm th}$ of each of the transistors on ROs. However, our method proposed in Sec. III successfully estimates the characteristics of the transistors by the measurement data on ROs. Therefore, this method is chosen in this paper. Note that all measurement data are taken from a single chip to eliminate chip-to-chip process variations.

Fig. 5 shows the timing chart to measure the frequency fluctuation in a single RO. It periodically repeats oscillations and pauses. Embedded counters are used to measure the number of oscillations periodically during each oscillation period. The numbers of oscillations are dynamically fluctuated by RTN-induced $\Delta V_{\rm th}$. The measurement conditions are as follows. The number of ROs is 840, the number of the measurements on a single RO is 9,024, the time of one cycle is $\Delta t = 2.2$ ms, and the duration time is $t_{\rm total} = 20$ s. Those conditions are determined because of the limitation of our measurement facilities. The supply voltage is $V_{\rm dd} = 0.65$ V instead of nominal 1 V. Different frequencies are observed in a single RO at each cycle because of the RTN effects.

Eq. (7) is used to evaluate the RTN-induced frequency fluctuation.

$$\frac{\Delta F}{F_{\rm max}} = \frac{F_{\rm max} - F_{\rm min}}{F_{\rm max}} \tag{7}$$

Where, $F_{\rm max}$ and $F_{\rm min}$ are defined as the maximum and the minimum value among measured 9,024 frequencies, respectively. $\Delta F/F_{\rm max}$ in Eq. (7) represents the impact of RTN on the circuits.

Fig. 6 shows the measurement results of $\Delta F/F_{\rm max}$. X and Y axes denote standard normal quantile and $\Delta F/F_{\rm max}$,

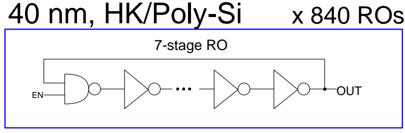

Fig. 4. Test structure to measure frequency fluctuation in 40 nm process.

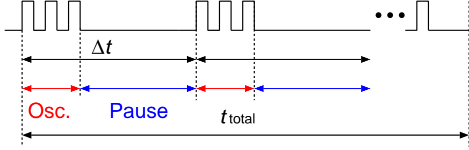

Fig. 5. Timing chart to measure RTN-induced frequency fluctuation.

respectively. RTN fluctuates the frequencies by 8.61% on 840 ROs. The frequencies of ROs are estimated to fluctuate 50% at the $+6\sigma$ point, if they follows the log-normal distribution. Practically, this estimation is inaccurate because the RTN-induced $\Delta V_{\rm th}$ follows the defect-centric distribution.

C. Circuit-Level RTN Prediction

To predict the RTN effects on the circuit-level, it is necessary that circuit simulation analyses with netlists including RTN-induced $\Delta V_{\rm th}$. The values of $\Delta V_{\rm th}$ are calculated by the transistor-level RTN model with the device characteristics. The distribution of the RTN effects is reproduced by a Monte Carlo analysis with such netlists.

Our goal is to replicate a distribution of the frequency fluctuations on measured ROs. Therefore, the device characteristics of the fabricated chip should be obtained. The RTN-induced $\Delta V_{\rm th}$ assumes to follow the bimodal defect-centric distribution because the chip is fabricated in the 40 nm SiON process. From this, it is necessary to estimate these four parameters, $N_{\rm HK}$, $N_{\rm IL}$, $\eta_{\rm HK}$, and $\eta_{\rm IL}$.

III. Estimation of Defect Characteristics and RTN Circuit Analysis

In this section, a method to estimate four defect characteristics of the bimodal defect-centric distribution from the measurement results of 840 ROs on the test chip are explained. We confirm that simulation results analyzed by using the parameters are matched with the measurement results

Fig. 7 shows an overview of algorithm to estimate the defect characteristics. Vectors of the threshold voltage shifts $\Delta\hat{V}_{\rm th}$ is calculated by using the bimodal defect-centric distribution with vectors of the defect characteristics $\hat{c}_i = (N_{\rm HK}, i, N_{\rm IL}, i, \eta_{\rm HK}, i, \eta_{\rm IL}, i)$. $\Delta\hat{V}_{\rm th}$ is converted to vectors of the frequency fluctuations $\Delta\hat{F}_{\rm sim}/F_{\rm max}$ by using sensitivities from prior circuit simulations. The KS test (Kolmogorov-Smirnov test) is performed between $\Delta\hat{F}_{\rm sim}/F_{\rm max}$ and the measure data $\Delta\hat{F}_{\rm meas}/F_{\rm max}$. The loops are repeated with manipulating $\hat{c}_i$ by the DS method (Downhill Simplex Method) until the probability value p_i from KS tests exceed $p_{\rm th}$ or the number of iterations exceed a limitation value $i_{\rm MAX}$. More details are introduced in later parts.

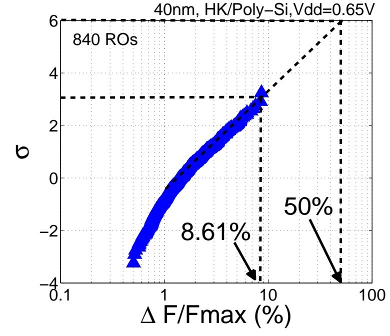

Fig. 6. Distribution of $\Delta F/F_{\rm max}$ of ring oscillators on 40 nm process.

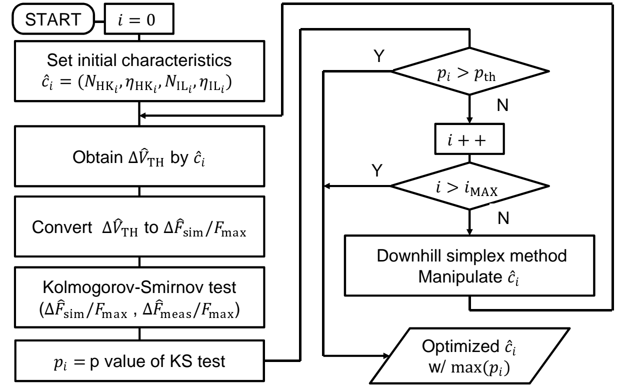

Fig. 7. Algorithm to estimate defect characteristics.

A. Analysis of Sensitivity of Frequency Fluctuation to Threshold Voltage Shift

Prior to the descriptions of the algorithm in Fig. 7, the sensitivity analyses of $\Delta F/F_{\rm max}$ to $\Delta V_{\rm th}$ is introduced. It is necessary to obtain the effect of RTN to circuit frequencies, nevertheless the circuit simulations take a lot of time. Therefore, the sensitivity is analyzed for efficient execution of the algorithm.

The relation between $\Delta F/F_{\rm max}$ of ROs and $\Delta V_{\rm th}$ on each of the MOSFETs is introduced. The frequency fluctuations by the MOSFETs ΔF_i are expressed as Eq. (8).

$$\Delta F_i \approx k_i \Delta V_{{\rm th},i} \tag{8}$$

Where, $\Delta V_{{\rm th},i}$ and k_i are the threshold voltage shift on the MOSFET and the sensitivity of ΔF_i to $\Delta V_{{\rm th},i}$, respectively. The sensitivity is changed by the supply voltage, the circuit structure, and so on. However, the sensitivities of each stage in ROs are assumed to be the same because the inverters are connected serially. $\Delta F/F_{\rm max}$ is described as Eq. (9).

$$\begin{aligned} \Delta F/F_{\rm max} &= \frac{1}{F_{\rm max}} \sum \Delta F_{{\rm INV},i} \\ &= \frac{1}{F_{\rm max}} \sum (k_{\rm n}\Delta V_{{\rm thn},i} + k_{\rm p}\Delta V_{{\rm thp},i}) \end{aligned} \tag{9}$$

Where, $\Delta F_{{\rm INV},i}$, $k_{\rm n}$, $k_{\rm p}$, $\Delta V_{{\rm thn},i}$, and $\Delta V_{{\rm thp},i}$ are the frequency fluctuations on each of the stages, the sensitivities on the single N/PMOSFETs, and $\Delta V_{\rm th}$ on ith N/PMOSFETs,

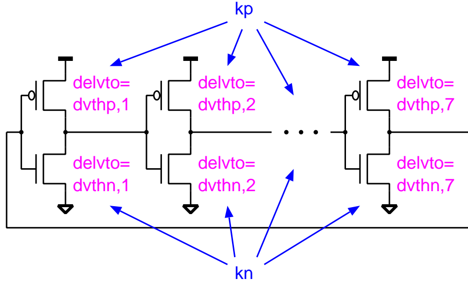

Fig. 8. Threshold voltage shift of each MOSFET (dvthn,i and dvthp,i) and sensitivity of NMOS and PMOS (k_n and k_p).

TABLE I
SIMULATION CONDITION.

Tr. model	40 nm HK/Poly-Si Standard
Cell Size	N/PMOS $L/W = 44/88$
Supply Voltage	0.65 V

respectively. Fig. 8 depicts k_n, k_p, $\Delta V_{\mathrm{thn},i}$, and $\Delta V_{\mathrm{thp},i}$. Note that delvto is the parameter of ΔV_th in BSIM. Hence, $\Delta F/F_\mathrm{max}$ can be calculated by ΔV_th if k_n and k_p of the circuits are already known.

Fig. 9 shows the simulation structure (the RO). It replicates the measurement circuit shown in Sec. II except the NAND is replaced by the inverter. The simulation conditions are summarized in Table I. $|\Delta V_\mathrm{th}|$ of a single N/PMOSFET in the RO is sweeped from 0 to 5 mV. Note that the impacts of RTN on ΔV_th are assumed to a few mV order ranges in the 40 nm process. ΔV_th of each of the MOSFETs are shifted in order to match the measurement and simulation results.

Fig. 10 shows analysis results. X and Y axes denote $|\Delta V_\mathrm{th}|$ and $\Delta F/F_\mathrm{max}$, respectively. Both results follow linear functions. Discrete fluctuations are caused by the SPICE model. Fitting functions of the results are expressed as Eqs. (10, 11).

$$f(\Delta V_\mathrm{thn}) = 0.7719 \times \Delta V_\mathrm{thn} \quad (10)$$
$$g(\Delta V_\mathrm{thp}) = 1.782 \times \Delta V_\mathrm{thp} \quad (11)$$

Asymptotic standard errors are 0.589% and 0.265%, respectively. The defect characteristics is estimated with those approximations.

B. Set Initial Vector of Defect Characteristics

The details of the vectors of the defect characteristics $\hat{c}_i$ are introduced. Each of the defects has four parameters, N_HK, η_HK, N_IL, and η_IL. In this method, a 5×4 matrix is made as the initial simplex. Each of the vertexes is $\hat{c}_i$.

The initial $\hat{c}_i$ are defined as follows to converge computation.

1) Read $\mu_{\Delta \mathrm{V_{th}}}$ (mean values of ΔV_th) from the measurement results
2) Determine provisional values of the defect characteristics

$\mu_{\Delta \mathrm{V_{th}}}$ is read by Fig. 6. When $\Delta V_{\mathrm{thn},i} = \Delta V_{\mathrm{thp},i} = \mu_{\Delta \mathrm{V_{th}}}$, then $\Delta F/F_\mathrm{max} = \mu_{\Delta F/F_\mathrm{max}}$ in Eq. (9). In this case, $\mu_{\Delta \mathrm{V_{th}}}$ is

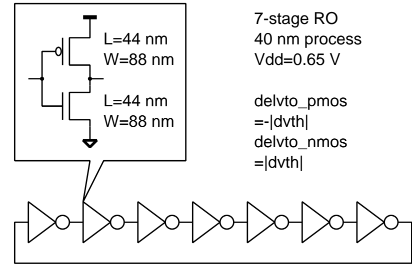

Fig. 9. Simulation structure.

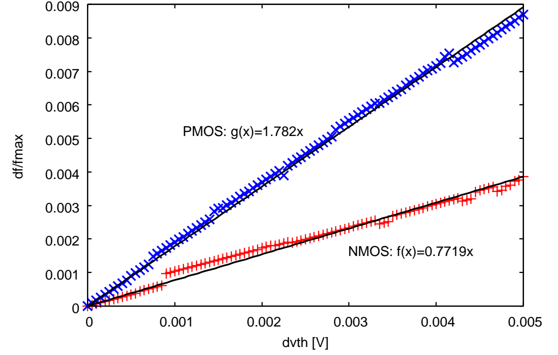

Fig. 10. Sensitivity of frequency fluctuation to threshold voltage shift.

expressed as Eq. (12).

$$\mu_{\Delta \mathrm{V_{th}}} = \mu_{\Delta F/F_\mathrm{max}}/i \times (k_\mathrm{n} + k_\mathrm{p}) \quad (12)$$

As shown in the section II, in the defect-centric distribution, $\mu_{\Delta \mathrm{V_{th}}}$ and $\sigma_{\Delta \mathrm{V_{th}}}$ are formulated in Eq. (4,5), respectively. If $\mu_{\Delta \mathrm{V_{th}}}$ is the sum of the mean values of ΔV_th on the HK and the IL, $\mu_{\Delta \mathrm{V_{th,HK}}}$ and $\mu_{\Delta \mathrm{V_{th,IL}}}$, respectively, Eq. (13) is established.

$$\begin{aligned} \mu_{\Delta \mathrm{V_{th}}} &= \mu_{\Delta \mathrm{V_{th,HK}}} + \mu_{\Delta \mathrm{V_{th,IL}}} \\ &= N_\mathrm{HK}\eta_\mathrm{HK} + N_\mathrm{IL}\eta_\mathrm{IL} \end{aligned} \quad (13)$$

Where, $\mu_{\Delta \mathrm{V_{th,HK}}} : \mu_{\Delta \mathrm{V_{th,IL}}} = 1:1$ is assumed. Empirically, the values of N_HK and η_IL are a digit and a few mV order. The initial vertexes (provisional values of the defect characteristics) are calculated in the above conditions.

C. Obtain Vectors of Threshold Voltage Shift and Frequency Fluctuation

The details of the vectors of the threshold voltage shifts $\Delta \hat{V}_\mathrm{th}$ is explained. $\Delta \hat{V}_\mathrm{th}$ is obtained by calculating $840 \times n_\mathrm{tr}$ times of ΔV_th with the defect-centric distribution $\hat{c}$, where $n_\mathrm{tr} = 14$ is the number of MOSFETs in the RO. $\Delta \hat{V}_\mathrm{th}$ reproduces the RTN-induced ΔV_th of each of the MOSFETs. In this method, the defect characteristics of the N/PMOSFETs are assumed to be equivalent. However, it has been reported that the characteristics of N/PMOSFETs are different. This is a subject of future investigation.

The details of the vectors of the frequency fluctuations $\Delta \hat{F}_\mathrm{sim}/F_\mathrm{max}$ is introduced. The measurement results are incomparable with $\Delta \hat{V}_\mathrm{th}$ because those are data of the values of

frequencies. Therefore, $\Delta\hat{V}_{\rm th}$ is converted to $\Delta\hat{F}_{\rm sim}/F_{\rm max}$ by using Eq. (9) with $k_{\rm n}$ and $k_{\rm p}$ obtained by the prior analyses.

D. Perform Kolmogorov-Smirnov Test Using Vector of Frequency Fluctuation and Measurement Data

The two-sample KS test determines that two samples are similar or not. It is the hypothesis test that evaluates the difference between CDFs of the distributions of the two sample data vectors over the range of x in each of the set. The test uses the value in Eq. (14) which is the maximum absolute difference between the CDFs of the distributions of the two vectors.

$$D^* = \max_x(|\hat{P}_1(x) - \hat{P}_2(x)) \tag{14}$$

Where, $\hat{P}_1(x)$ and $\hat{P}_2(x)$ are the proportions of x_1 and x_2 values less than or equal to x, respectively. In the test, the decision to reject the null hypothesis "two data are from the same continuous distribution" is based on comparing the p_i value with the significance-level. If p_i is larger than the significance-level, two samples are assumed to have the most similar distribution. The tests are performed using $\Delta\hat{F}_{\rm meas}/F_{\rm max}$ and $\Delta\hat{F}_{\rm sim}/F_{\rm max}$, then p_i for $\hat{c}_i$ are identified.

E. Manipulate Vector of Defect Characteristics by Downhill Simplex Method

The DS method is one of the solutions for optimization problems of multidimensional variables. In this method, the minimum value of the objective function is achieved by manipulating vertexes of the simplex repeatedly. The method has four ways of the standard manipulation called reflection, expansion, reduction, and contraction. $(N+1)$-dimensional simplex is used for the N-dimensional function, hence, 5-dimensional simplex is set. The vertexes and the function values are $\hat{c}_i$ and $1-p_i$, respectively. Therefore, the simplex consists of a 4×5 matrix.

The convergence condition is $1-p_i < p_{\rm th}$. Added to this, $i_{\rm MAX}$ is the maximum iteration. If any $1-p_i$ does not exceed $p_{\rm th}$, $\hat{c}_i$ with the maximum $1-p_i$ is regarded as the estimation result.

F. Estimation Results of Defect Characteristics and Prediction of RTN Effect

The distribution of RTN-induced frequency fluctuations are reproduced by the Monte Carlo simulation with the defect characteristics obtained by the method proposed in this section.

The estimation result is ($N_{\rm HK}$, $\eta_{\rm HK}$, $N_{\rm IL}$, $\eta_{\rm IL}$)=(4.00, 0.121 mV, 0.142, 3.17 mV). Conditions of the estimation are $p_{\rm th} = 99\%$ and $i_{\rm MAX} = 1000$. The circuits and conditions are as same as those shown in Fig. 9 and Table I. $\Delta V_{\rm th}$ is calculated by the defect-centric distribution with the result. The distribution of the frequency fluctuations are analyzed by 840 times Monte Carlo circuit simulations.

Figs. 11 and 12 shows the distributions of measured $\Delta\hat{F}_{\rm meas}/F_{\rm max}$ and predicted $\Delta\hat{F}_{\rm sim}/F_{\rm max}$ by the estimated $\hat{c}$, respectively. X and Y axes are $\Delta F/F_{\rm max}$ and standard normal quantile, respectively. Matching between the results is confirmed.

IV. Conclusion

We propose the circuit analysis method using the bimodal defect-centric distribution on the 40 nm SiON process and the method to estimate the defect characteristics. The RTN-induced variations should be taken into account, but the conventional unimodal model is fails to replicate the effects on 40 nm or later processes. The proposed method uses the bimodal model which has the parameters corresponding to two dielectric layers. To predict the distribution of the RTN-induced frequency fluctuations, the method to estimate the defect characteristics by the measurement data is proposed. The RTN-induced variations on the test chip are accurately reproduced by using the Monte Carlo analysis.

References

[1] B. Kaczer, J. Franco, P. J. Roussel, G. Groeseneken, T. Chiarella, N. Horiguchi, and T. Grasser, "Extraction of the Random Component of Time-Dependent Variability Using Matched Pairs," *IEEE Electron Device Letters*, vol. 36, no. 4, pp. 300–302, April 2015.

[2] T. Matsumoto, K. Kobayashi, and H. Onodera, "Impact of random telegraph noise on CMOS logic circuit reliability," in *IEEE CICC*, Sept. 2014, pp. 1–8.

[3] B. Kaczer, T. Grasser, P. Roussel, J. Franco, R. Degraeve, L. A. Ragnarsson, E. Simoen, G. Groeseneken, and H. Reisinger, "Origin of nbti variability in deeply scaled pfets," in *IEEE IRPS*, 2010, pp. 26–32.

[4] K. Ito, T. Matsumoto, S. Nishizawa, H. Sunagawa, K. Kobayashi, and H. Onodera, "The Impact of RTN on Performance Fluctuation in CMOS Logic Circuits," in *IRPS*, Apr. 2011, pp. CR.5.1–CR.5.4.

[5] K. H. Joo, C. R. Moon, S. N. Lee, X. Wang, J. K. Yang, I. S. Yeo, D. Lee, O. Nam, U. I. Chung, J. T. Moon, and B. I. Ryu, "Novel Charge Trap Devices with NCBO Trap Layers for NVM or Image Sensor," in *IEDM*, Dec 2006, pp. 1–4.

[6] H. Kurata, K. Otsuga, A. Kotabe, S. Kajiyama, T. Osabe, Y. Sasago, S. Narumi, K. Tokami, S. Kamohara, and O. Tsuchiya, "Random Telegraph Signal in Flash Memory: Its Impact on Scaling of Multilevel Flash Memory Beyond the 90-nm Node," *IEEE JSSC*, vol. 42, no. 6, pp. 1362–1369, June 2007.

[7] M. Yamaoka, H. Miki, A. Bansal, S. Wu, D. J. Frank, E. Leobandung, and K. Torii, "Evaluation methodology for random telegraph noise effects in SRAM arrays," in *IEDM*, Dec 2011, pp. 32.2.1–32.2.4.

[8] B. Kaczer, C. Chen, P. Weckx, P. Roussel, M. Toledano-Luque, J. Franco, M. Cho, J. Watt, K. Chanda, G. Groeseneken, and T. Grasser, "Maximizing reliable performance of advanced cmos circuits—a case study," in *IEEE IRPS*, June 2014, pp. 2D.4.1–2D.4.6.

[9] A. Oshima, P. Weckx, B. Kaczer, K. Kobayashi, and T. Matsumoto, "Impact of Random Telegraph Noise on Ring Oscillators Evaluated by Circuit-level Simulations," in *ICICDT*, June 2015.

[10] P. Weckx, B. Kaczer, C. Chen, J. Franco, E. Bury, K. Chanda, J. Watt, P. J. Roussel, F. Catthoor, and G. Groeseneken, "Characterization of time-dependent variability using 32k transistor arrays in an advanced HK/MG technology," in *IRPS*, 2015, pp. 3B.1.1–3B.1.6.

[11] A. Oshima, T. Komawaki, K. Kobayashi, R. Kishida, P. Weckx, B. Kaczer, T. Matsumoto, and H. Onodera, "Physical-Based RTN Modeling of Ring Oscillators in 40-nm SiON and 28-nm HKMG by Bimodal Defect-Centric Behaviors," in *SISPAD*, Sept. 2016, pp. 327–330.

[12] M. Toledano-Luque, B. Kaczer, J. Franco, P. Roussel, T. Grasser, T. Hoffmann, and G. Groeseneken, "From mean values to distributions of BTI lifetime of deeply scaled FETs through atomistic understanding of the degradation ," in *VLSIT*, June 2011, pp. 152–153.

[13] K. Takeuchi, T. Nagumo, S. Yokogawa, K. Imai, and Y. Hayashi, "Single-charge-based modeling of transistor characteristics fluctuations based on statistical measurement of RTN amplitude," in *VLSIT*, June 2009, pp. 54–55.

[14] H. Nakamura, Y. Nakahara, N. Kimizuka, T. Abe, I. Yamamoto, T. Fukase, T. Nakayama, K. Taniguchi, K. Masuzaki, K. Uejima, T. Iwamoto, T. Tatsumi, and K. Imai, "55nm CMOS Technology for Low Standby Power/Generic Applications Deploying the Combination

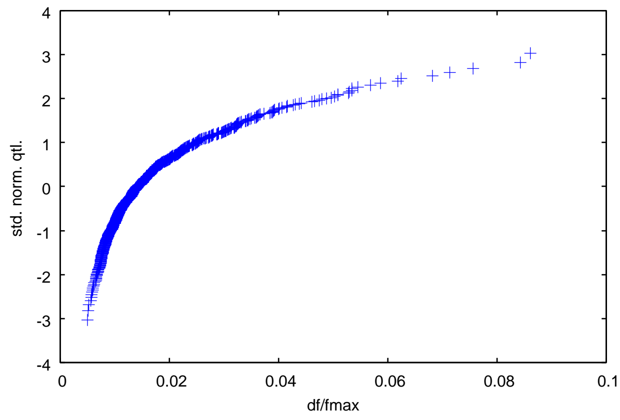

Fig. 11. Distribution of measured $\Delta\hat{F}_{\mathrm{meas}}/F_{\mathrm{max}}$.

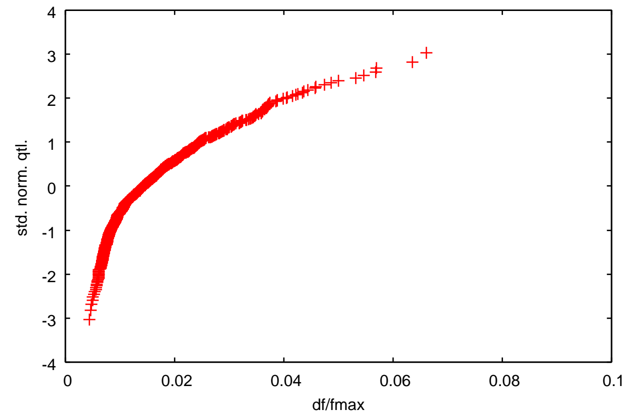

Fig. 12. Distribution of predicted $\Delta\hat{F}_{\mathrm{sim}}/F_{\mathrm{max}}$ by estimated defect characteristics.

of Gate Work Function Control by HfSiON and Stress-Induced Mobility Enhancement," in *VLSIT*, 2006, pp. 158–159.